Self-consistent cluster-embedding calculation method and the calculated electronic structure of NiO

Haoping Zheng
Department of Physics and Astronomy, Louisiana State University, Baton Rouge, Louisiana 70803
(Received 5 April 1993; revised manuscript received 6 July 1993)

The self-consistent cluster-embedding method is discussed theoretically. A definition of the total energy for an embedded cluster has been introduced. The method has two advantages. (i) It can describe both localized and band properties, including their excitations. (ii) It can give a good description of the magnetic properties for both spin-ordered and spin-disordered states. The electronic structure of NiO is studied using a high-quality basis set to calculate the electronic structure of a small embedded cluster and an antiferromagnetic insulating ground state is obtained. The picture has both localized and band properties. A small energy gap separates the unoccupied and occupied nickel $3d$ orbitals which are well localized. Each $3d$ orbital is attached to a particular nickel ion. Below the $3d$ levels are two diffuse oxygen $2p$ bands, and above the $3d$ levels are oxygen $3s$, nickel $4s$, and oxygen $3p$ bands. Experimental data concerning photoemission and optical absorption can be interpreted naturally. The spin magnetic moment of the nickel ion is calculated correctly. The simulation of the spin-disordered state shows that NiO remains as an insulator in the paramagnetic state. The Néel temperature of NiO is calculated directly to give a reasonable result. The Hubbard U parameter for nickel $3d$ electrons is estimated. The calculation shows that the excited nickel $3d$ electrons are also well localized and the overlaps are less than 4.5%. We propose the following: The overlap of the excited $3d$ electrons is too small to form a metallic band, but the overlap is sufficient for the "hole" to migrate through the crystal. In this sense, NiO is a charge-transfer insulator with a gap of about 4 eV (mostly from oxygen to nickel). The calculated small energy gap (about 0.5 eV) provides the activation energy of NiO which is supported by the experimental results.

I. INTRODUCTION

A cluster model has been used to study localized physical phenomena in ionic solids. A major problem in this approach is how to simulate the effect of the crystal environment on a cluster so the cluster can represent a portion of a solid. This is referred to as "embedding." A procedure in which the cluster is surrounded by many point charges has been used in cluster calculations by many authors.[1–5] Its explicit purpose is to keep the total system electrically neutral and to reproduce the ionic crystal field. However, the potential produced by the point charge array is not accurate except where the point charge is far away from the cluster. Use of point charges for embedding forces one to restrict the basis used in the calculation: A diffuse basis set may make the electrons localize on the point charges which leaves the results totally meaningless.[2] However, if diffuse functions are not employed, the calculated unoccupied orbitals are usually not correct and sometimes the valence electron orbitals are effected because of the lack of diffuse basis.[5]

A self-consistent embedded-cluster model has been proposed by Ellis, Benesh, and Byrom.[6] In this model, the *crystal charge density* is constructed by extending the cluster charge density periodically. The "collapse disaster" is prevented by truncating the deep core potentials (which surround the cluster) to a constant, thus introducing one empirical parameter. This model has been used to study the electronic structure and the magnetic properties of a variety of metallic, semiconducting, and insulating materials.[7–9] The method presented here is the same as that of Ellis except for some technical details. In this paper, we give the method a theoretical discussion from the viewpoint of total energy. It is found that although there is an empirical parameter, this self-consistent cluster-embedding method is accurate if some conditions are satisfied. A definition of the total energy for the embedded cluster is introduced, which makes this method useful in studying the magnetic properties, especially the spin-disordered state. The main restriction of this method is that the electron hybridization is limited to the cluster atoms. So the calculated eigenvalues are discrete. Inglesfield's embedding approach[10] has no such drawback, but it requires knowing the Green function of crystal in advance.

For the past 50 years, the insulating nature of the transition-metal monoxides has been a continuing problem for the condensed-matter physics community. NiO has been extensively studied previously. Early investigations of the properties of NiO are summarized in a review by Adler and Feinleib.[11] Various theoretical calculations have been performed. Controversy still exists. The essential question is what model furnishes a reasonable starting point for describing the properties of NiO. Spin-polarized energy-band calculations have given some correct answers for the ground-state properties of NiO.[12–15] But it failed to give a correct magnetic moment of a nickel ion. Besides, the predicted energy gap is too small. Mott, Hubbard, and Anderson have argued that the one-electron approximation breaks down for these transition-metal monoxides because of strongly correlated $3d$ electrons.[16–18] Mott illustrated that the

simple band picture breaks down and a gap opens when the Coulomb interaction parameter is larger than the bandwidth.[17] A systematic description of the Mott insulators has been given by Brandow.[19] Recently, Fujimori and Minani[20,21] and Sawatzky and Allen[22] have given another picture of NiO: The empty upper Hubbard $3d$ band and the filled lower Hubbard $3d$ band separated by the Coulomb energy U. The oxygen band resides in between these two $3d$ bands and forms a charge-transfer gap with the upper $3d$ band.

NiO is believed to have both localized and band properties.[23] It is an antiferromagnet. An accurately embedded cluster calculation in which a high-quality basis set is employed has two advantages. (i) This method can describe both localized and band properties, including their excitations. (ii) This method can give a good description of the magnetic properties for both spin-ordered and spin-disordered state. Here, we use a high-quality basis set for a four-atom embedded cluster to calculate the electronic structure of NiO. The results show a success: the dual properties and the magnetic properties of NiO are well described. Based on the results, we proposed a new explanation to the insulating nature of NiO.

This paper is organized in the following way. Section II gives a theoretical model. The basic formulas are derived for the self-consistent cluster-embedding method. Section III gives a computational procedure. Section IV gives calculated results for a two-atom Ni-O cluster. Section V gives calculated results of a four-atom Ni_2O_2 cluster and its comparison with the experimental data.

II. THEORETICAL MODEL

In this section a theoretical discussion of the self-consistent cluster-embedding method is given. The central problem is how to distinguish the cluster electrons from the background electrons without changing the total energy of the system.

The ground-state energy functional of N interacting electrons and M nuclei can be written in the form[24]

$$E_G[\rho]=T[\rho]+E_{\rm xc}[\rho]+\int\int\frac{\rho(\mathbf{r})\rho(\mathbf{r}')}{|\mathbf{r}-\mathbf{r}'|}d\mathbf{r}\,d\mathbf{r}' -2\sum_{i=1}^{M}\int\frac{\rho(\mathbf{r})Z_i}{|\mathbf{r}-\mathbf{R}_i|}d\mathbf{r}+\sum_{\substack{ij\\ i\neq j}}^{M}\frac{Z_iZ_j}{|\mathbf{R}_i-\mathbf{R}_j|}\ . \tag{2.1}$$

Atomic units are used throughout this paper ($e^2=2$, $\hbar=1$, $2m_e=1$). The local spin-density approximation means

$$E_{\rm xc}[\rho]=\int\rho(\mathbf{r})\epsilon_{\rm xc}(\rho^{\rm up}(\mathbf{r}),\rho^{\rm down}(\mathbf{r}))d\mathbf{r}\ , \tag{2.2}$$

where the function $\epsilon_{\rm xc}$ is taken from the exchange-correlation energy density of a uniform interacting electron system. $T[\rho]$ and $\rho(\mathbf{r})$ have the following forms:

$$\rho(\mathbf{r})=\rho^{\rm up}(\mathbf{r})+\rho^{\rm down}(\mathbf{r})=\sum_{\sigma}\sum_{\text{occupied }l}|\Phi_l^{\sigma}(\mathbf{r})|^2\ , \tag{2.3}$$

$$T[\rho]=\sum_{\sigma}\sum_{\text{occupied }l}\int\Phi_l^{\sigma *}(\mathbf{r})(-\nabla^2)\Phi_l^{\sigma}(\mathbf{r})d\mathbf{r}\ . \tag{2.4}$$

At the present time, we do not include relativistic effects. By varying the ground-state energy with respect to $\Phi_k^{\sigma *}(\mathbf{r})$ under the conservation rule, $\delta\int\rho(\mathbf{r})d\mathbf{r}=0$, the Kohn-Sham equations are obtained:[25]

$$\left\{-\nabla^2+2\int\frac{\rho(\mathbf{r}')}{|\mathbf{r}-\mathbf{r}'|}d\mathbf{r}'-2\sum_{i=1}^{M}\frac{Z_i}{|\mathbf{r}-\mathbf{R}_i|}+V_{\rm xc}^{\sigma}(\mathbf{r})\right\}\Phi_k^{\sigma}(\mathbf{r}) =\lambda_k^{\sigma}\Phi_k^{\sigma}(\mathbf{r})\ , \tag{2.5}$$

where the exchange-correlation potential $V_{\rm xc}^{\sigma}(\mathbf{r})$ is

$$V_{\rm xc}^{\sigma}(\mathbf{r})=\frac{\partial}{\partial\rho^{\sigma}(\mathbf{r})}(\rho(\mathbf{r})\epsilon_{\rm xc})\ . \tag{2.6}$$

A. Full potential embedding

We separate the N electrons into N_1 electrons and N_2 electrons, and the M nuclei into M_1 nuclei and M_2 nuclei, where N_1 and M_1 refer to the cluster and N_2 and M_2 to the background. Since all exchange-correlation energy is expressed explicitly in $E_{\rm xc}[\rho]$, the distinguishing of electrons should not change the total energy. If $\rho_1(\mathbf{r})$ is the charge density of N_1 electrons, and $\rho_2(\mathbf{r})$ is the charge density of N_2 electrons, the total ground-state energy (2.1) can be rewritten as

$$E_G[\rho_1+\rho_2]=T[\rho_1]+T[\rho_2]+\int\int\frac{[\rho_1(\mathbf{r})+\rho_2(\mathbf{r})][\rho_1(\mathbf{r}')+\rho_2(\mathbf{r}')]}{|\mathbf{r}-\mathbf{r}'|}d\mathbf{r}\,d\mathbf{r}' +E_{\rm xc}[\rho_1+\rho_2]-2\sum_{i=1}^{M}\int\frac{[\rho_1(\mathbf{r})+\rho_2(\mathbf{r})]Z_i}{|\mathbf{r}-\mathbf{R}_i|}d\mathbf{r}+\sum_{i\neq j}^{M}\frac{Z_iZ_j}{|\mathbf{R}_i-\mathbf{R}_j|}\ . \tag{2.7}$$

Suppose we already know the charge density $\rho_2(\mathbf{r})$. Apply (2.3) and (2.4) to ρ_1 and $T[\rho_1]$. By varying $E_G[\rho_1+\rho_2]$ with respect to $\phi_k^{\sigma *}(\mathbf{r})$ under the conservation rule $\delta\int\rho_1(\mathbf{r})d\mathbf{r}=0$, we get the new Kohn-Sham equation:

$$\left\{-\nabla^2+2\int\frac{\rho_1(\mathbf{r}')+\rho_2(\mathbf{r}')}{|\mathbf{r}-\mathbf{r}'|}d\mathbf{r}'-2\sum_{i=1}^{M}\frac{Z_i}{|\mathbf{r}-\mathbf{R}_i|}+V_{\rm xc}^{\sigma}(\mathbf{r})\right\}\phi_k^{\sigma}(\mathbf{r})=\lambda_k^{\sigma}\phi_k^{\sigma}(\mathbf{r})\ . \tag{2.8}$$

Equation (2.8) can be solved only if the surrounding charge density $\rho_2(\mathbf{r})$ is already known. In the crystal, $\rho_2(\mathbf{r})$ can be

obtained by using the periodicity. If we choose the primary cell of the crystal as our cluster, $\rho_1(\mathbf{r})$ as its charge density, then

$$\rho_2(\mathbf{r})=\sum_{\alpha\neq 0}\rho_1(\mathbf{r}-\mathbf{R}_\alpha)\ , \tag{2.9}$$

where $\mathbf{R}_0=\mathbf{0}$ is the origin of the cluster. The summation is over all surrounding cells.

The total ground-state energy E_G is proportional to the number of cells. We need a formula to represent the energy of a cell. This formula should satisfy two requirements: For an arbitrary system which contains k cells, if the energy of each cell is represented by the formula, then (i) the total ground-state energy is equal to the sum of the energy of each cell; (ii) for a crystal, if k goes to infinity, the energies of all cells converge to a same value of E_G/k. For a system containing two electrons, each electron has half of the total interaction energy. Using this idea and separating $E_{\rm xc}[\rho_1+\rho_2]$ into

$$\begin{aligned}E_{\rm xc}[\rho_1+\rho_2]&=\int\sum_\sigma(\rho_1^\sigma+\rho_2^\sigma)\epsilon_{\rm xc}((\rho_1+\rho_2)^{\rm up},(\rho_1+\rho_2)^{\rm down})d\mathbf{r}\\&=\int\sum_\sigma\rho_1^\sigma\epsilon_{\rm xc}(\rho^{\rm up},\rho^{\rm down})d\mathbf{r}+\int\sum_\sigma\rho_2^\sigma\epsilon_{\rm xc}(\rho^{\rm up},\rho^{\rm down})d\mathbf{r}\\&\equiv E_{\rm xc1}[\rho_1,\rho_2]+E_{\rm xc2}[\rho_1,\rho_2]\ ,\end{aligned}$$

we get

$$E_G[N,M]=E_1[N_1,M_1]+E_2[N_2,M_2]\ ,$$

where

$$E_1[N_1,M_1]=T[\rho_1]+E_{\rm xc1}[\rho_1,\rho_2]+\int\int\frac{\rho_1(\mathbf{r})\rho_1(\mathbf{r}')}{|\mathbf{r}-\mathbf{r}'|}d\mathbf{r}\,d\mathbf{r}'+\int\int\frac{\rho_1(\mathbf{r})\rho_2(\mathbf{r}')}{|\mathbf{r}-\mathbf{r}'|}d\mathbf{r}\,d\mathbf{r}'-2\sum_{i=1}^{M}\int\frac{\rho_1(\mathbf{r})Z_i}{|\mathbf{r}-\mathbf{R}_i|}d\mathbf{r}\ . \tag{2.10}$$

E_2 has the same form as E_1 except for exchange of ρ_1 and ρ_2. Fixed nuclei were assumed and the Coulomb interaction energy between the nuclei was removed (for a fixed lattice, this is a constant). The definition (2.10) has no effect on the calculation. But the accurate representation of the energy of the embedded cluster makes this method useful in the study of magnetic structure.

B. Orthogonality constraint

Unfortunately, formulas (2.8) and (2.9) cannot give correct results. The electrons of the cluster atoms collapse into the core region of surrounding atoms, making the result totally meaningless. In Eq. (2.8), all potentials produced by surrounding M_2 atoms are exactly the same as in Eq. (2.5), so why do Eqs. (2.8) and (2.5) give different results? Actually, Eqs. (2.8) and (2.9) together are not equivalent to the original Kohn-Sham equation (2.5). Using Eq. (2.5), the electron wave functions of all M atoms will orthogonalize with each other. But using Eqs. (2.8) and (2.9), only the electron wave functions of M_1 atoms in the cluster will orthogonalize with each other. No electron wave functions of surrounding atoms appear in Eq. (2.8). The separation of the cluster electrons from the background electrons and the absence of the "orthogonality constraint" to the surrounding M_2 atoms caused the collapse. To our knowledge, there is no analytic theory of the "orthogonality." We need to find a way to simulate the property of the orthogonality at least in the atomic core region. In the core region of an atom, all electron orbitals are filled, the core is "hard," which means it is difficult for additional electrons to get into the "hard core."

Instead of the wave function used in pseudopotential arguments, we try to discuss this problem from the viewpoint of the total energy. Here we introduce our basic assumption: "The possibility of an electron of cluster atoms getting into the hard core of surrounding atoms is almost zero." First, a new equation is derived from this assumption. Then we discuss the physical meaning of the assumption.

If $\rho_1(\mathbf{r})$ is the charge density of the cluster, then the assumption can be expressed mathematically as

$$\rho_1(\mathbf{r})|_{\mathbf{r}\text{ in core }j}=0\ , \tag{2.11}$$

where $j=1,2,\ldots,M_2$, indicating the core regions of all surrounding atoms. Suppose there is a potential $V_{\rm or}$:

$$V_{\rm or}=\begin{cases}2\displaystyle\sum_{j=1}^{M_2}(Z_j/|\mathbf{r}-\mathbf{R}_j|) & \text{if } \mathbf{r} \text{ is in the core of surrounding atoms}\ ,\\ 0 & \text{otherwise}\ .\end{cases} \tag{2.12}$$

Combining (2.11) and (2.12), we get

$$\rho_1(\mathbf{r})V_{\rm or}(\mathbf{r})=0 \tag{2.13}$$

in whole space. So we can add a term $\int V_{\rm or}(\mathbf{r})\rho_1(\mathbf{r})d\mathbf{r}$ into the right side of Eq. (2.7) without changing the total ground-state energy E_G. If we write Eq. (2.8) as

$$H^\sigma\phi_k^\sigma(\mathbf{r})=\lambda_k^\sigma\phi_k^\sigma(\mathbf{r}) , \tag{2.14}$$

by using same variation method, we finally get a new equation:

$$\{H^\sigma+V_{\rm or}\}\phi_k^\sigma(\mathbf{r})=\lambda_k^\sigma\phi_k^\sigma(\mathbf{r}) . \tag{2.15}$$

The question is, does Eq. (2.15) imply Eq. (2.11), i.e., is our basic assumption self-consistent? Actually, the potential $V_{\rm or}$ cancels the nuclear Coulomb potential in the core regions of all surrounding atoms (not including cluster atoms). Cluster electrons will only feel an electron-electron positive Coulomb potential in these areas and be forced out. The results of our calculation show, for a cluster with 36 electrons, that only a total of 0.0006 electrons remains in all core regions of the surrounding 116 atoms. So Eqs. (2.11) and (2.13) are satisfied very accurately, which means the ground-state energy E_G can still be calculated by Eq. (2.7) and $V_{\rm or}$ has no contribution to the ground-state energy. We call $V_{\rm or}$ the "orthogonality constraint." Equations (2.15) and (2.9) are the basic formulas of our calculation.

We have proved that if our basic assumption is correct, Eq. (2.15) will give a correct charge density and $V_{\rm or}$ will have no contribution to the ground-state energy. Now the key point is, is our basic assumption reasonable? Figure 1 can help us to explain the situation more clearly. Apparently, the potentials (nucleus-electron Coulomb potential, electron-electron Coulomb potential, and the exchange-correlation potential) produced by both cluster atoms and surrounding atoms in the whole blank area of Fig. 1 are exact. The orthogonality constraint prevents the cluster electrons from getting into the dashed area which represents the cores of the surrounding atoms. We believe this is a good approximation to the real solid. A simple argument is as follows. For a real solid, one additional electron that gets into a filled core means that one original electron gets out of the core. The indistinguishability of electrons makes the core unchanged, i.e., the core is "hard." But in the cluster-embedding calculation, ρ_1 is distinguished from ρ_2. The only way for the hard core to remain unchanged is to prevent ρ_1 from getting into it.

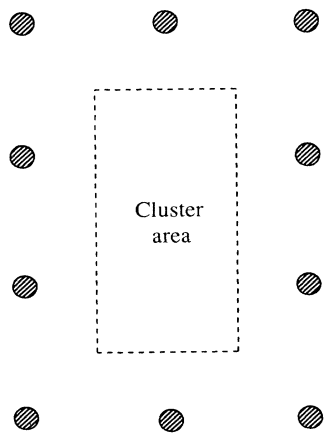

FIG. 1. Cluster area and the surrounding atomic cores.

One important conclusion can be obtained from the above discussion: whatever the core radius is, the formula (2.7) for the total ground-state energy remains valid provided that the condition (2.11) is satisfied. The only effect of increasing the core radius is that ρ_1 is pushed further away from the surrounding nuclei. Compared with the total volume, the change of core volume caused by a reasonable change of core radius is very small. This explains why the calculated results are not sensitive to the core radius if the system is not in a "collapsed" state. In this sense, the self-consistent embedded-cluster method is accurate if the condition (2.11) is satisfied. In the next section, we will see, by using two simple rules, that the core radius can be actually well determined.

Apparently, the choice of $V_{\rm or}$ is not unique. We choose definition (2.12), so the force which pushes the ρ_1 out of core comes from the core charge density ρ_2. Consequently, the ρ_1 which is near the core is effected by the core charge density ρ_2. Our choice is similar to that used by Ellis.[6,9] They treat this problem by truncating the deep core potentials (which surround the cluster) at an energy V_F to a constant. Usually $V_F=E_F$, the Fermi energy. It is found that the change of V_F over a reasonable range has very little effect on calculated properties.[6,9]

The embedding approach is actually a kind of electron charge renormalization. It separates the cluster electrons from the background electrons under the condition that the total energy of the system is unchanged. It also preserves the localized and spread properties of the charge distribution in the cluster. The main restriction of this method is that the calculated eigenvalues are discrete because the number of atoms in a cluster is finite.

In conclusion, the following points have been emphasized: In the whole blank area of Fig. 1, the potentials are exact. The orthogonality constraint $V_{\rm or}$ keeps the ρ_1 out of the dashed area. $V_{\rm or}$ itself has no contribution to the ground-state energy. We believe such a charge density ρ_1 is a good approximation to the real solid.

III. COMPUTATIONAL PROCEDURE

A general program package for the embedded-cluster system has been developed by the present author based on the general free-cluster program package developed by Chen.[26] The local-spin-density-approximation Kohn-Sham equation (2.15) is solved self-consistently. Beginning with the trial charge density ρ_1 of free atoms, the charge density ρ_2 of the surrounding atoms is obtained by using Eq. (2.9). Then the trial Hamiltonian H^σ and $V_{\rm or}$ are attained. After solving Eq. (2.15), the eigenfunctions $\phi_k^\sigma(\mathbf{r})$ are used to build the new charge densities ρ_1 and ρ_2, and the next iteration begins. We discuss several points in detail.

A. Cluster

From Eq. (2.15), it is apparent that the eigenvalues are determined by the total potential $\{H^\sigma + V_{or}\}$. Unlike the free cluster, the point symmetry of an embedded cluster is of much less importance to the eigenvalues because the surrounding atoms can provide almost the same potentials as the cluster atoms. This will be discussed further in Sec. V A. In order to avoid the approximate density decomposition (according to Mulliken populations) and to keep crystal stoichiometry, clusters like Ni_nO_n are chosen. Since disk-storage space is limited, there are two choices: Use a small basis set to calculate a relatively large cluster, or use a high-quality basis set to calculate a small cluster. In this paper, we prefer the latter since a high-quality basis set is crucial to investigating both localized and extended properties of NiO and to getting reliable excited states. NiO is an antiferromagnet. Because of the superexchange effect, we should calculate at least a four-atom embedded cluster which is actually the maximum size our computer can afford. A two-step method is used because of the lack of disk-storage space. In the first step, a two-atom Ni-O embedded cluster is calculated with the self-consistent determination of the surrounding charge density. The purpose of this step is to obtain the charge density ρ_1, and to study the direct exchange-correlation effect. In the second step, a four-atom Ni_2O_2 embedded cluster is calculated with fixed surrounding charge density ρ_2. Initially, ρ_2 is built from ρ_1 of the first step. Then ρ_2 is built from ρ_1 of the new result of the four-atom Ni_2O_2 cluster again and again. Self-consistency is reached roughly in this repetitive way. All properties of solid NiO are obtained from this step.

B. Basis

The linear combination of Gaussian orbitals (LCGO) are used as the basis function. Table I gives our basis set, which was originally provided by Wachters[27] and van Duijneveldt.[28] The nickel $3d$ bases were reoptimized by Rappe, Smedley, and Goddard III.[29] For oxygen, a d polarization function was used.[30] The use of the orthogonality constraint makes it possible to use a high-quality basis set, which is crucial to the calculation. Compared with the original basis, 4 exponents have been inserted and 19 diffuse exponents have been added. The smallest exponent is 0.0095, which enables the basis to reach up to seventh nearest atom. The ratios between added adjoining exponents is about 2. In order to reduce the size of the Hamiltonian matrix, two nickel s, one nickel p, and one oxygen s bases remain as contracted bases (they represent mostly the inner electrons). All other bases are uncontracted. A small change of the basis set tested in a two-atom-cluster calculation only caused less than 0.03-eV energy differences. We considered this to be an adequate indication of convergence.

C. Core region of surrounding atoms

The orthogonality constraint V_{or} of Eq. (2.12) is evaluated numerically in each core region of the surrounding atoms. Because all inner orbitals are filled, the core region has a spherical shape. In the core regions, we multiply V_{or} by a function f which is almost a step function (see Fig. 2). The only purpose of f is to keep the continuity of the potential at the point r_0. The cutoff radius r_0 is adjusted according to two simple rules: (i) avoid numerical instability; (ii) keep total energy minimum. In practice, adjusting r_0 is simple. When r_0 is too small, "collapse" occurs, the total energy becomes much lower, and there are many negative Mulliken population numbers which show instability. Increasing r_0 will increase the total energy (ρ_1 is pushed away from the surrounding nuclei) and decrease the number of negative Mulliken populations. When all orbitals have physically meaningful Mulliken populations, the adjusting is finished so the total energy is at a minimum. We call this value of r_0 an optimum value which gives the best quality of the potential produced by the surrounding atoms. There is still some empirical character to the optimum choice of r_0. Our experience shows that when r_0 is a little larger or smaller than the optimum value, the order of energy levels remains the same. There are some small shifts of orbital energies, mostly in the same direction. This actually does not change the general picture.

D. Two fitting procedures

In order to avoid the calculations of enormous numbers of four-center, two-electron integrals, two fitting procedures have been used.[26] One is the charge-density fitting:

$$\rho^\sigma(\mathbf{r}) \approx \sum_k a_{k\sigma} f_k(\mathbf{r}) , \tag{3.1}$$

where f_k is the fitting basis. We used spherical Gaussian functions of s type ($e^{-\alpha r^2}$) and r^2 type ($r^2 e^{-\alpha r^2}$) centered at each atom. The fitting coefficients $a_{k\sigma}$ were evaluated analytically by a variational procedure which minimizes the errors in electrostatic energy. The second is exchange-correlation potential fitting:

$$V_{xc}^\sigma(\mathbf{r}) \approx \sum_l b_{l\sigma} f_l(\mathbf{r}) . \tag{3.2}$$

The fitting basis functions are the same as in (3.1). Numerical integrations were performed to determine the least-squares-fitting coefficients. We use the von Barth

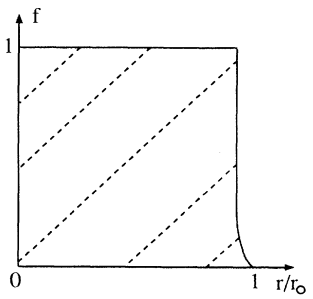

FIG. 2. The f function.

and Hedin[31] form of the exchange-correlation potential, as parametrized by Rajagopal and co-workers.[32]

Because ρ_1 is almost zero in the core region of surrounding atoms, we use the approximation

$$E_{\mathrm{xc1}}[\rho_1,\rho_2]=\int \rho_1\epsilon_{\mathrm{xc}}(\rho^{\mathrm{up}},\rho^{\mathrm{down}})d\mathbf{r}$$
$$\approx \int \rho_1\epsilon_{\mathrm{xc}}(\rho_1^{\mathrm{up}},\rho_1^{\mathrm{down}})d\mathbf{r} \quad (3.3)$$

TABLE I. Basis set of (a) a nickel atom and (b) an oxygen atom.

(a)

Original	Our basis $S(11)$ Exponent	Coefficient	Original	Our basis $P(10)$ Exponent	Coefficient
same	284 878.0	3.200×10^{-4}	same	1774.18	2.9500×10^{-3}
same	419 97.9	2.460×10^{-3}	same	423.403	2.3370×10^{-2}
same	962 7.67	1.254×10^{-2}	same	138.311	1.0406×10^{-1}
same	276 1.96	4.926×10^{-2}	same	53.1703	2.8226×10^{-1}
same	920.488	1.495×10^{-1}	same	22.3874	4.3486×10^{-1}
same	341.805	3.264×10^{-1}			
			same	9.928 48	1.0000
same	138.023	4.0474×10^{-1}	same	4.116 25	1.0000
same	59.2 587	1.9186×10^{-1}	same	1.710 31	1.0000
			same	0.672 528	1.0000
same	20.3 712	1.0000		0.170 446	1.0000
same	8.59 400	1.0000		0.083 145	1.0000
same	2.39 417	1.0000		0.040 558	1.0000
same	0.918 169	1.0000		0.019 785	1.0000
	0.205 000	1.0000		0.009 651	1.0000
0.130 176	0.129 199	1.0000			
0.046 392	0.060 093	1.0000			
	0.027 950	1.0000			
	0.013 000	1.0000			

$d(12)$

	Exponent	Coefficient		Exponent	Coefficient
same	58.730 0	1.0000		0.342 741	1.0000
same	16.710 0	1.0000	0.1825	0.173 980	1.0000
same	5.783 00	1.0000		0.088 315	1.0000
2.064	2.826 482	1.0000		0.044 830	1.0000
	1.381 463	1.0000		0.022 756	1.0000
same	0.675 200	1.0000		0.011 551	1.0000

(b)

Original	Our basis $S(11)$ Exponent	Coefficient	Original	Our basis $P(13)$ Exponent	Coefficient
same	105 374.95	$1.430\,0\times10^{-4}$	same	200.000 00	1.0000
same	15 679.240	$1.123\,0\times10^{-3}$	same	46.533 367	1.0000
same	3 534.544 7	$5.980\,0\times10^{-3}$	same	14.621 809	1.0000
same	987.365 16	$2.556\,2\times10^{-2}$	same	5.313 064	1.0000
same	315.978 75	$9.259\,0\times10^{-2}$	2.102 525	2.667 525	1.0000
same	111.654 28	$2.817\,49\times10^{-1}$		1.339 281	1.0000
same	42.699 451	$6.771\,64\times10^{-1}$	0.850 223	0.672 412	1.0000
			same	0.337 597	1.0000
same	17.395 596	1.0000	0.128 892	0.171 369	1.0000
same	7.438 309	1.0000		0.086 989	1.0000
same	3.222 862	1.0000		0.044 157	1.0000
same	1.253 877	1.0000		0.022 415	1.0000
same	0.495 155	1.0000		0.011 378	1.0000
same	0.191 665	1.0000			
	0.090 435	1.0000			
	0.042 671	1.0000		$d(1)$	
	0.020 134	1.0000			
	0.009 500	1.0000	same	1.154 000	1.0000

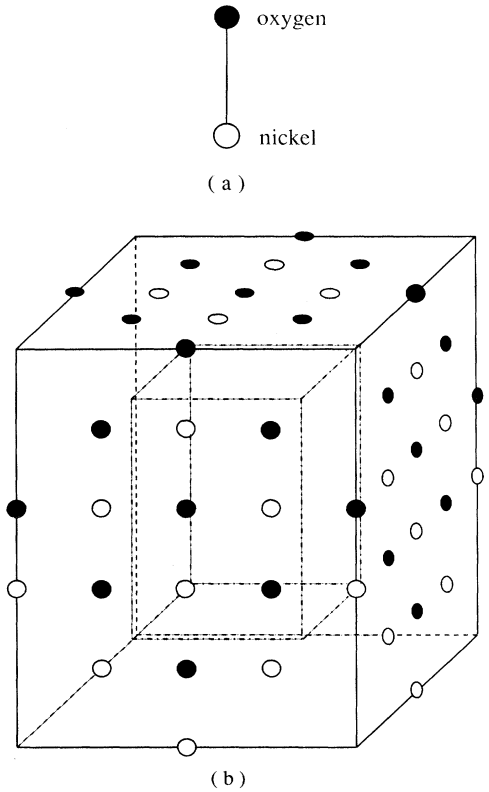

FIG. 3. (a) Two-atom cluster. (b) 116 surrounding atoms.

in these regions. The results actually remain the same, but the CPU time is reduced by about one-third.

IV. RESULTS OF THE TWO-ATOM CLUSTER

Figure 3(a) shows the two-atom Ni-O cluster structure. Figure 3(b) shows the surrounding 116 Ni and O atoms. The lattice constant used in our calculation is 4.1684 Å, which is the value of the lattice constant in crystalline NiO.[33] When an atom is far away from the cluster, we can use a point charge to approximate its potential. An ionic embedding procedure was used here.[3] Total 5084 point charges filling a $17\times17\times18$ cuboid are used. The point charges were placed on atomic sites which surround the Ni-O cluster and 116 atoms. The location of the embedding charges were those of the true crystal structure. $+2|e|$ charges were put on Ni sites, $-2|e|$ charges on O sites. On the outmost boundary, fractional ($\frac{1}{2}$, $\frac{1}{4}$, and $\frac{1}{8}$) charges were put on the faces, edges, and corners. This arrangement makes the Madelung constant on a nickel atom and an oxygen atom in the cluster equal to 1.747 565, the same as the exact Madelung constant of an ionic crystal with the sodium chloride structure.[34] The orthogonality constraint is applied to both surrounding atoms and point charges. Here is the question: is this arrangement a good representation of the crystalline environment? An investigation on this question has been done. Table II gives the calculated electronic structure properties with respect to the number of surrounding atoms. Table III gives the calculated electronic structure properties with respect to the number of point charges. Both tables show a satisfactory degree of convergence when 116 atoms and 5084 point charges are used. We expect that the 116 atoms and 5084 point charges will produce an accurate solid potential in the cluster area.

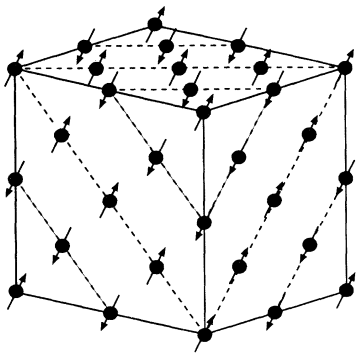

FIG. 4. Magnetic structure of NiO. Only Ni ions are shown in the diagram.

The total number of basis functions is 156. The total number of fitting bases is 64. After several trial calculations, we find that the optimum values of the cutoff radii of Ni and O atoms are 0.369 and 1.131 a.u., respectively. The total cluster electrons remaining in the surrounding core regions are 0.0006 electron, which means condition (2.11) is well satisfied. In the calculation of V_{or}, 1376 points and 2494 points are used for the nickel core and the oxygen core, respectively. A total of 183 720 points filling the big cuboid in Fig. 3(b) are used in the calculation of V_{xc}. In general, after 60 self-consistent-field (SCF) iterations the total energy can achieve the accuracy of 10^{-7} Ry. So we can compare the energy difference in units of K.

Table IV shows the results with antiferromagnetic structure. The antiferromagnetic structure of NiO, according to neutron-diffraction experiments,[35] is shown in Fig. 4. It is easy to arrange the atomic spin directions of

TABLE II. The convergence test with respect to the number of surrounding atoms. (Two-atom cluster. The total number of surrounding atoms and the point charges are 5200.)

Number of surrounding atoms	E_f (Ry)	Energy gap (eV)	Width of Ni 3d bands (eV)	Energy gap between Ni 3d bands and O 2p bands (eV)
44	−0.3186	0.398	2.08	0.75
100	−0.3292	0.212	2.27	1.32
116	−0.3302	0.204	2.27	1.30

TABLE III. The convergence test with respect to the number of point charges. (Two-atom cluster. The total number of surrounding atoms is 116.)

Number of point charges	Madelung constant	E_f (Ry)	Energy gap (eV)	Width of Ni 3d bands (eV)	Energy gap between Ni 3d bands and O 2p bands (eV)
2248	1.747 568	−0.3491	0.212	2.26	1.31
3482	1.747 563	−0.3387	0.208	2.27	1.29
5084	1.747 565	−0.3302	0.204	2.27	1.30

surrounding atoms in our calculation. In density-functional theory, only two spin directions are considered: up and down. Our spin-polarized calculation produces two charge densities: ρ^{up} and ρ^{down}. Note, no spatial direction is assigned to "up" or "down." As an approximation, we define the atomic spin direction in the sense of electron spin direction: If $\int \rho^{\text{up}} d\mathbf{r}$ is larger than $\int \rho^{\text{down}} d\mathbf{r}$, the atom has up atomic spin direction. The exchange of ρ^{up} and ρ^{down} implies a change of the atomic spin direction. When we construct the background charge density ρ_2 in each surrounding cell, we can easily choose the atomic spin direction by exchanging the ρ_1^{up} and ρ_1^{down}. The disadvantage of this definition is that each atom has only two atomic spin directions. This will not effect the calculation of ferromagnet and antiferromagnet. But for a disordered state, this is an approximation. When we calculate the disordered state, the spin-up atoms and the spin-down atoms are chosen randomly by a random-number-generating subroutine under the condition that the number of spin-up atoms should be close to the number of spin-down atoms. Table V gives our results. All results are calculated self-consistently. No magnetic interaction appears in our calculation. The difference of total energy is caused purely by the exchange-correlation interaction. In general, the total energy is determined by 12 second nearest nickel ions (to the cluster-Ni atom). Because of the $0.03\mu_B$ unphysical spin magnetic moment of the oxygen ion and the diffuse property of the charge density, there is a big effect coming from the six nearest oxygen ions (to the cluster-Ni atom) and the six nearest nickel ions (to the cluster-O atom). The conclusion is that the parallel spin magnetic moment lowers the total energy and the antiparallel spin magnetic moment raises the total energy. To explain this result, we note that the cluster contains only one Ni atom. Only direct exchange-correlation energy between cluster atoms and the surrounding atoms is included. This result implies that the antiferromagnetic structure of NiO is not formed by the direct exchange-correlation effect.

V. RESULTS OF THE FOUR-ATOM CLUSTER

Figure 5 shows the four-atom Ni_2O_2 cluster. The surrounding atoms and ionic embedding procedure used here is similar to Sec. IV. The number of surrounding atoms is 124. The number of point charges is 5380, which makes the Madelung constant at the positions of cluster atoms equal to 1.747 565, as in Sec. IV. From the test results of Sec. IV, we expect that the 124 atoms and 5380 point charges will produce an accurate solid potential in the cluster area. The total number of basis functions is 312. The total number of fitting functions is 128. The cutoff radii of surrounding Ni and O atoms are the same as in Sec. IV. A total of 240 096 points are used in the V_{xc} calculation. Initially, the charge density ρ_2 of the surrounding atoms is built from ρ_1 (the result of Sec. IV) according to antiferromagnetic structure, and is fixed during the calculation. After 60 SCF (only involving ρ_1; ρ_2 is fixed) calculations, the ρ_1 of the four-atom cluster reaches an accuracy of 10^{-7} Ry with respect to the fixed ρ_2. Then we use this calculated new ρ_1 to build the new ρ_2 and to calculate the next result. This repetitive method is so time consuming that we can barely reach the self-consistency. Actually, after four of these "iterations," the differences of all eigenvalues are less than 0.0015 Ry, the difference of the total energy is less than 0.005 Ry, and the unphysical spin magnetic moment of the oxygen ion is reduced to less than $3\times10^{-8}\mu_B$. We think this result is acceptable. In this section, all background charge densities ρ_2 are built from the same ρ_1 and are fixed during the calculation. The SCF iteration is only with respect to ρ_1.

A. Cluster ground state

We build ρ_2 from ρ_1 according to the antiferromagnetic structure. After 60 SCF iterations, the total energy has an accuracy of 10^{-7} Ry. There are 0.000 98 cluster electrons remaining in the surrounding core regions, which means condition (2.11) is well satisfied. Table VI gives

TABLE IV. Results of the two-atom Ni-O cluster with antiferromagnetic structure.

Fermi energy (Ry)	Energy gap (eV)	Width of Ni 3d bands (eV)	Energy gap between Ni 3d bands and O 2p bands (eV)	Spin magnetic moment (μ_B)
−0.3302	0.204	2.27	1.30	1.97

TABLE V. Results of the two-atom Ni-O cluster with different atomic spin direction arrangement of surrounding atoms.

No.	Atomic spin direction arrangement	12 second nearest Ni atoms para.	anti.	Total energy (relative to the fifth row) (K)
1	all spin up (58 up, 0 down)	12	0	−36
2	disordered 1 (29 up, 29 down)	9	3	−19
3	disordered 2 (29 up, 29 down)	8	4	−3
4	disordered 3 (29 up, 29 down)	7	5	+6
5	antiferromag. (29 up, 29 down)	6	6	0
6	disordered 4 (31 up, 27 down)	6	6	+5
7	disordered 5 (29 up, 29 down)	5	7	+28
8	disordered 6 (29 up, 29 down)	4	8	−15
9	all spin down (0 up, 58 down)	0	12	+4

the eigenvalues and Mulliken populations of spin-up orbitals. The spin-down orbitals are the same as the spin-up orbitals except for the exchanging of atom 1 and atom 2. We have paid special attention to the nickel $3d$ electrons and oxygen $2p$ electrons: the Mulliken populations of two nickel atoms and two oxygen atoms have been shown separately. The Mulliken population analysis yields the spin magnetic moment of $1.91\mu_B$ for the nickel ion, which is in agreement with the experimental data of $1.77\mu_B$,[36] $1.64\mu_B$,[37] and $1.90\mu_B$.[38] The energy-band calculation gives $1.04\mu_B$.[12,15] Terakura *et al.* believe that the deviations are from the spherical-potential approximation used in the band-structure calculation.[15]

The general picture is as follows. A 0.51-eV energy gap separates the unoccupied and occupied nickel $3d$ orbitals which are well localized. Each $3d$ orbital is attached to a particular nickel ion. Below the $3d$ levels are two diffuse oxygen $2p$ bands. Above the $3d$ levels are oxygen $3s$, nickel $4s$, and oxygen $3p$ bands. Our picture is different from Svane and Gunnarsson,[39] but similar to that of Terakura *et al.* except for two differences. Figure 6(a) shows the total density of states of NiO according to the spin-polarized energy-band calculation done by Terakura *et al.*[15] Figure 6(b) shows our calculated eigenvalues. The six nickel orbital groups (two unoccupied, four occupied) are very similar to the results of Terakura *et al.* Both small energy gaps, 0.51 and 0.2 eV,[12] do not agree with the experimental data of 4 eV.[22,40] An explanation of this discrepancy will be given in Sec. V E. There are two differences between our results and that of Terakura *et al.*: (i) the relative positions of two oxygen $2p$ bands are different, which will be discussed in Sec. V C; (ii) our results have both localized and band properties. The Mulliken populations show that each $3d$ orbital is attached to one nickel atom, but each $2p$ orbital is shared by two oxygen atoms (see Table VI). Besides the Mulliken populations, a "charge overlap" is used to describe localized and band properties. The charge overlap between two orbitals i and j is defined as follow:

$$(\text{Charge Overlap})_{ij} = \int \min(\rho_i(\mathbf{r}),\rho_j(\mathbf{r}))d\mathbf{r} \ . \quad (5.1)$$

Unless otherwise specified, the "overlap" in this paper means charge overlap. The overlap between two orbitals of type 36 (orbital 36, spin up, attached to Ni_2; orbital 36, spin down, attached to Ni_1) is 2.98%. In contrast, the overlap between two orbitals of type 28 (orbital 28, spin up, 80% shared by two oxygen atoms and 17% of Ni_1; orbital 28, spin down, 80% shared by two oxygen atoms and 17% of Ni_2) is 84.48%. The overlap between two or-

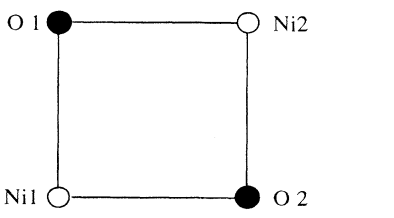

FIG. 5. Four-atom Ni_2O_2 cluster.

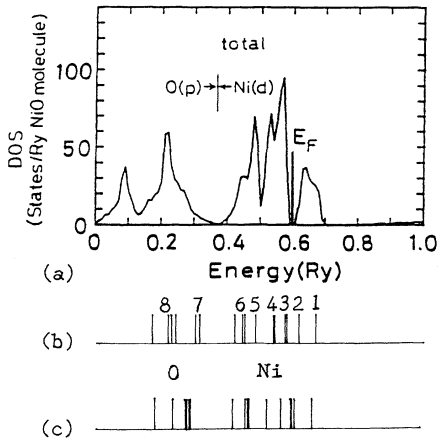

FIG. 6. (a) The total state density of NiO obtained by the spin-polarized energy-band calculation (Ref. 15). (b) Eigenvalues of the embedded Ni_2O_2 cluster. (c) Eigenvalues of the embedded Ni-O-Ni-O cluster.

bitals of type 39 (oxygen 3*s* electrons) is 96.07%. This means each 3*d* electron is well localized and attached to a particular nickel atom, while the oxygen 2*p* and 3*s* electrons are shared by all oxygen atoms and form the bands. As we will see, the coexistence of both localized and band properties is very important in understanding NiO.

As expected, the result is an antiferromagnetic insulating state. There is an energy gap of 0.51 eV. Two nickel ions have opposite spin magnetic moments and two oxygen ions have no spin magnetic moment, so the total magnetic moment of the cluster Ni_2O_2 is zero. Section IV has proved that the direct exchange-correlation effect between two nickel atoms can only make two spins parallel. But we get a spin antiparallel state. A reasonable explanation is the 90° "superexchange effect": the electronic wave functions of two nickel ions are coupled through the intermediate oxygen ions.[41,42] Here we want to emphasize that the 90° superexchange effect at least does not

TABLE VI. Eigenvalues and Mulliken populations of Ni_2O_2 cluster in ground state (spin-up orbitals).

Orbital	No.	Energy (Ry)	Ni *s*	Ni *p*	Ni_1 *d*	Ni_2 *d*	O *s*	O_1 *p*	O_2 *p*
O 3*p*	44	0.6349		0.01	−0.01	−0.01		0.51	0.51
(Ni 4*p*)	43	0.5959		0.43	−0.04	−0.04		0.32	0.32
Ni 4*s*	42	0.4737	0.77	0.07	−0.02	−0.01	−0.28	0.23	0.23
	41	0.4459	1.05	−0.25	−0.03	−0.03	−0.01	0.14	0.14
O 3*s*	40	0.2540		−0.20	−0.04	−0.04	1.10	0.10	0.10
	39	0.1534	0.05	−0.11	−0.01	−0.02	1.08		
Ni 3*d*	38	−0.2740				0.93	0.02	0.02	0.02
	37	−0.3243	0.01		0.01	0.97	−0.01	0.01	0.01
		above are the unoccupied orbitals							
Ni 3*d*	36	−0.3618 (E_f)				0.97		0.01	0.01
	35	−0.3669	0.01		0.01	0.95		0.01	0.01
	34	−0.4014				0.95		0.03	0.03
	33	−0.4033		0.01	0.88	0.01	0.02	0.05	0.05
	32	−0.4583	0.01		0.96	0.02	−0.01	0.01	0.01
	31	−0.4912			0.93			0.04	0.04
	30	−0.5001	0.02		0.94	0.01		0.02	0.02
	29	−0.5236			0.82	0.02		0.08	0.08
O 2*p*	28	−0.6278			0.17	0.03		0.40	0.40
	27	−0.6424			0.07	0.02		0.46	0.46
	26	−0.7025		0.03		0.04	0.03	0.45	0.45
	25	−0.7149		0.01	0.09		0.04	0.43	0.43
	24	−0.7228	0.17	−0.06	0.04	0.01		0.43	0.43
	23	−0.7744	0.15	0.05	0.01		−0.09	0.44	0.44
O 2*s*	22	−1.7033		−0.02			1.01	0.01	0.01
	21	−1.7119	−0.05	−0.03			1.05	0.01	0.01
Ni 3*p*	20	−4.7990		1.00					
	19	−4.8446		1.00					
	18	−4.8819		1.00					
	17	−4.9503		1.00					
	16	−4.9927		1.00					
	15	−5.0300		1.00					
Ni 3*s*	14	−7.5430	1.00						
	13	−7.6960	1.00						
O 1*s*	12	−37.2385					1.00		
	11	−37.2385					1.00		
Ni 2*p*	10	−61.4159		1.00					
	9	−61.4204		1.00					
	8	−61.4252		1.00					
	7	−61.4817		1.00					
	6	−61.4858		1.00					
	5	−61.4907		1.00					
Ni 2*s*	4	−70.2378	1.00						
	3	−70.3242	1.00						
Ni 1*s*	2	−595.5220	1.00						
	1	−595.5230	1.00						

occur in the highest three occupied nickel $3d$ orbitals (orbitals 36, 35, and 34, since their hybridizations with oxygen ions are less than 6%), which have the same spin direction as two unoccupied nickel $3d$ orbitals. In order to study the 180° superexchange effect, the embedded cluster Ni-O-Ni-O is calculated. Because of the small difference of the environments between two nickel atoms, the energy levels of two nickel ions are slightly different and the converging is difficult. By freezing the occupation numbers and using a very small damping factor, a roughly converged result is finally obtained. The eigenvalues of ions with lower levels are shown in Fig. 6(c). Only some general conclusions can be confirmed. (i) The general picture of the eigenvalue structure is the same as the cluster Ni_2O_2. (ii) The dual property (both localized and band properties) is the same as the cluster Ni_2O_2. (iii) As was the case for the 90° superexchange effect, the 180° superexchange effect at least does not occur in the highest three occupied nickel $3d$ orbitals (orbitals 36, 35, and 34, since their hybridizations with oxygen ions are less than 3%), which have the same spin direction as the two unoccupied nickel $3d$ orbitals. The cluster Ni-O-Ni-O will not be discussed further. Compared with the results of the two-atom cluster, the results for the cluster Ni_2O_2 show some interesting changes. (i) The energy gap is increased from 0.204 to 0.51 eV. (ii) The spin magnetic moment of each nickel ion is decreased from $1.97\mu_B$ to $1.91\mu_B$. (iii) The Fermi energy is lowered from -0.3302 to -0.3618 Ry. (iv) The width of Ni $3d$ bands becomes a little smaller, the width of oxygen $2p$ bands becomes larger. All these changes make the results better compared with the experimental data. Actually, our results show that the superexchange effect between two nickel ions doubles the unit cell and reduces the energies of the occupied orbitals.

As mentioned in Sec. III, there is a symmetry problem: the eigenvalues in Table VI do not show the point symmetry of solid NiO. From Eq. (2.15), we know that the eigenvalues are determined by the total potential. Three factors can break the point symmetry of the total potential. (i) Antiferromagnetism. For a nickel ion, if we consider only the 6 nearest oxygen ions, the potential will have the point symmetry of solid NiO. But if we consider the 12 second nearest nickel ions, the exchange-correlation potentials are different for two spin parallel nickel ions and for two spin antiparallel nickel ions. (ii) The cluster does not have the point symmetry of NiO. For an ion in the cluster, four nearest ions have an orthogonality-constraint term and two other nearest ions (in the cluster) are automatically orthogonalized. This leads to a small difference in the potential. (iii) For each ionic shell in the cluster, beginning from the seventh nearest atoms, some ions are replaced by point charges. Actually, the core orbitals show roughly the point symmetry of solid NiO because the first two factors have less of an effect on them. Comparing Figs. 6(b) and 6(c), we can see that the geometric difference of the cluster does not change the general eigenvalue picture.

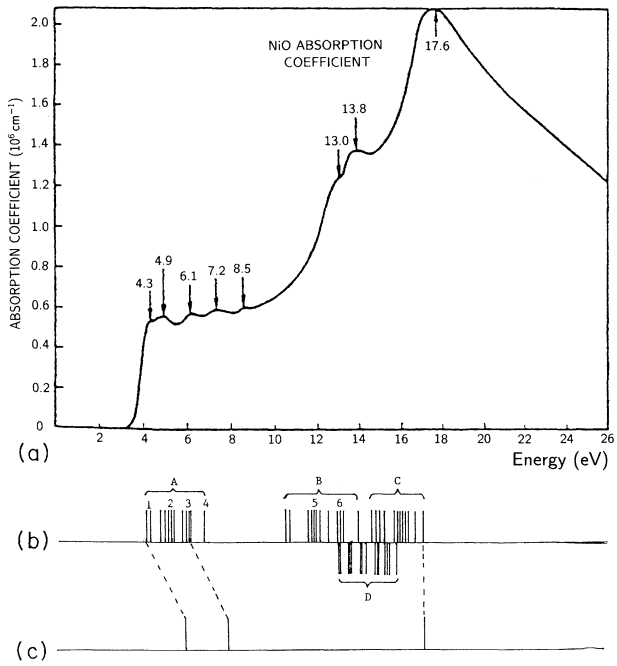

FIG. 7. (a) The experimental results of the optical-absorption coefficient of NiO (Ref. 46). (b) The optically allowed transition energies obtained by using the eigenvalues. (c) Three transition energies obtained by the transition-state method. Each dashed line connects the same transitions.

B. Optically allowed transitions

We believe use of a high-quality basis set combined with the accurately embedded cluster makes the first several unoccupied orbitals acceptable. This provides a good interpretation for the experimental optical-absorption coefficient.

Because ρ_2 is fixed and the electron rearrangement of ρ_1 is limited by ρ_2, the transition energy obtained by the Slater transition-state method[43–45] is higher than the real value (the limitation of rearrangement raises the energy). On the other hand, the transition energy obtained by using eigenvalues is lower than the real value with an error of second order in the derivative of the total energy. In order to estimate the real value, we use both the eigenvalues and the transition-state method to get the optically allowed transition energies. Figure 7(a) shows the experimental results for the optical-absorption coefficient of NiO obtained by Powell and Spicer.[46] Figure 7(b) shows optically allowed transition energies obtained by using the eigenvalues. All optically allowed transitions, from nickel $3d$ and oxygen $2p$ valence orbitals to the unoccupied nickel $3d$, oxygen $3s$, nickel $4s$, and oxygen $3p$ orbitals, were included. The highest unoccupied orbital we count is an oxygen $3p$ orbital with an eigenvalue 0.6349 Ry (8.6 eV). Figure 7(c) shows our results according to the transition-state method. Because the transition-state calculation is very time consuming and sometimes is difficult to converge, only three transition energies have

been calculated.

Part *A* of Fig. 7(b) contains the transition energies from oxygen 2*p* orbitals to the unoccupied nickel 3*d* orbitals. These are charge-transfer transitions. Because the nickel 3*d* orbitals are localized and oxygen 2*p* orbitals are diffuse, transferring one oxygen 2*p* electron to an unoccupied nickel 3*d* orbital will cause large electron rearrangement. This caused a relatively big difference between Figs. 7(b) and 7(c) [the rearrangement is limited in Fig. 7(c), which raises the energy drastically]. Part *C* contains the energies from oxygen 2*p* orbitals to nickel unoccupied 4*s* orbitals. Because both orbitals are diffuse, the electron rearrangement is small and the difference between Figs. 7(b) and 7(c) is small (about 0.2 eV). This small difference implies that in part *A*, Fig. 7(b) is more reliable. We use Fig. 7(b) to interpret the experimental data and understand that the real value will be a little larger than that in Fig. 7(b) if the transition involves a large electron rearrangement.

Our picture is that the main absorption edge comes from the charge-transfer transitions between oxygen 2*p* orbitals and unoccupied nickel 3*d* orbitals (part *A*). Our calculated first transition energy (4.1 eV) in Fig. 7(b) gives the correct main absorption edge. The peaks around 13.0 and 13.8 eV come from the transitions between oxygen 2*p* orbitals and unoccupied oxygen 3*s* orbitals (part *B*). The 0.8-eV energy difference represents the energy difference between two oxygen 2*p* bands [see Fig. 6(b), groups 7 and 8]. The peak at 17.6 eV comes from two groups of transitions, oxygen 2*p* orbitals to unoccupied nickel 4*s* orbitals (part *C*), and nickel 3*d* orbitals to unoccupied oxygen 3*p* orbitals (hybridized with nickel 4*p* electron, part *D*).

The weak optical-absorption lines below the threshold are generally ascribed to dipole-forbidden transitions between 3*d* states of the same nickel ion. The localized property of 3*d* excitations will be shown in Sec. V E. By using the eigenvalues in Table VI, we can get ten 3*d*-3*d* transition groups. Their average values are (in eV) 0.55, 1.06, 1.23, 1.75, 1.82, 2.33, 2.51, 2.71, 3.02, and 3.40 eV. The experimental data between 1.0 and 3.4 eV are 1.1, 1.7, 1.9, 2.2, 2.7, 3.0, and 3.3 eV.[11] Apparently, they are close to each other. Besides, by using the eigenvalues, the nickel 3*p* to 3*d* threshold is 61 eV, which is close to the experimental result of 64 eV.

C. Photoemission spectra

Because of the reason mentioned in Sec. V B, we simply use the eigenvalues in Table VI as the ionization potential, which is believed to involve an error of the second order in the derivative of the total energy. Only relative energy differences are important.

Figure 8(a) shows the photoemission experimental data and the results of the energy-band calculation of NiO reported by Shen *et al.*[23] Figure 8(b) shows our calculated results. In general, our results are similar to the energy-band calculation. Both show that nickel 3*d* bands are higher above the oxygen 2*p* bands. The oxygen 2*p* bands are thought to agree relatively well with the experimental data; the nickel 3*d* bands are relatively poor compared with the data. The major difference is that the lowest calculated oxygen 2*p* band of Fig. 8(a), which corresponds to the lowest 2*p* peak in Fig. 6(a), is absent from our results. Photoemitted electrons coming from this band are not observed.

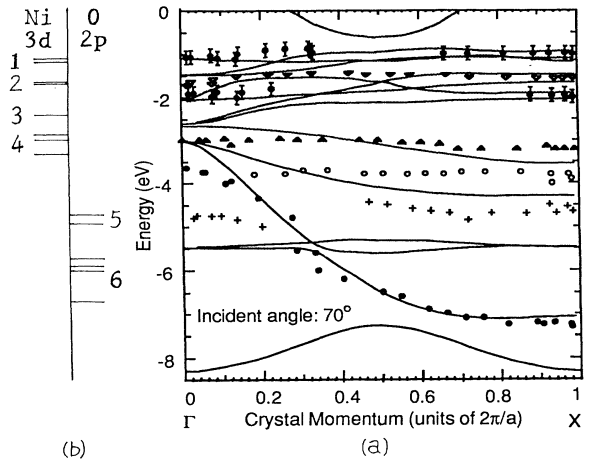

FIG. 8. (a) The photoemission experimental data and the results of an energy-band calculation (Ref. 23). (b) The eigenvalues of the embedded Ni_2O_2 cluster.

We interpret four spectral features (represented by Φ, ▼, ▲, and ○) as the nickel 3*d* orbital groups (1, 2, 3, and 4), and two spectral features (represented by † and ●) as the oxygen 2*p* bands (5 and 6). Ni 3*d* bands are narrow (groups 1, 2, and 3). Oxygen 2*p* bands are broad (group 6). Hybridized Ni 3*d*–O 2*p* levels have medium bandwidth (groups 4 and 5).

D. Magnetic properties

In order to estimate how stable the local antiferromagnetic state is, we need to obtain the ferromagnetic state. Actually, the ferromagnetic state is not stable in our calculation. If the damping factor is large, it will change to the antiferromagnetic state. Starting with the ferromagnetic charge density, we fix ρ_2 according to ferromagnetic structure and use a damping factor of 0.05; after 176 iterations we get an accuracy of 10^{-5} Ry. The total energy is 0.327 eV (3790 K) above the energy of the antiferromagnetic state. This energy difference is much higher than the Néel temperature, indicating a very stable local antiferromagnetic (AF) order. It is reasonable to assume that in a paramagnetic state, although the long-range AF order has been destroyed, local AF order still remains and the local moments of nickel ions persist essentially unchanged. This assumption is supported by many experimental observations.

Gubanov and Ellis have calculated the Néel temperature of NiO by the "magnetic transition-state" approach.[47] But there is no successful direct calculation of the Néel temperature. Here we assume that every two nickel ions are coupled together to form a pair with opposite spin directions, all pairs having the same charge density. In order to determine the antiferromagnetic structure and to calculate the Néel temperature directly, some geometrical restrictions are needed to "keep the lo-

cal AF pair." We assume (i) the total number of spin-up nickel ions should equal the total number of spin-down ions; (ii) in any cube (containing four nickel ions and four oxygen ions), the four nickel ions should not have the same spin direction. During the calculation, our four-atom cluster remains in AF order; the surrounding atomic spin directions are disordered. A random-number-generating subroutine is used to choose the spin-up atoms and the spin-down atoms. Then we apply two geometrical restrictions to the 18 nearest nickel ions (other nickel ions actually cannot change the result). Table VII gives our results. The total energies in Table VII are shown relative to the first row. The last two rows show the special cases which violate our restrictions. One has all spins up, the other has each cluster-nickel ion surrounded by spin-parallel nickel ions. Both cases cannot happen in practice because of the local AF order. Apparently, the antiferromagnetic structure has the lowest energy among the disordered structures. The disordered states are not completely disordered due to the local AF order, so the change of the system entropy may be not large. If we neglect the change of system entropy, by averaging the seven disordered results in Table VII, we get the Néel temperature 224 K. The experimental result is 525 K.[34] We think that the discrepancy results from our inability to include enough ions in our cluster, from the imperfection of the exchange-correlation potential we used, and from the neglect of the change of system entropy. To the best of our knowledge, this is the first direct calculation of the Néel temperature which gives a reasonable result.

Table VII also shows the energy gaps, the optical-absorption edges, and the spin magnetic moment of each nickel ion. It is clear that they are independent of the long-range spin order. Nickel ions have actually the same spin magnetic moment in all spin-disordered states as in the antiferromagnetic state, which shows the consistency of our assumption. We find that all spin-disordered states have the same electronic structure in the local AF pair as that of the antiferromagnetic state. From the discussion in the next subsection, we can say that NiO remains as an insulator when it transforms from antiferromagnetic to paramagnetic states. The real solid NiO is an insulator in both antiferromagnetic and paramagnetic phase.

E. Energy gap

In this subsection, we propose a new explanation of the insulating nature of NiO.

As in the case of the energy-band calculations, the main discrepancy between our theoretical calculation and experiments is the small energy gap. In order to give an alternative explanation, the Hubbard U parameter for the nickel $3d$ electron is estimated first. The ionization potential of orbital 36 and the electron affinity of orbital 37 were calculated by using the transition-state method. We take the point of view that U should be the difference between the ionization potential and the electron affinity. The result is $U_{dd} \approx 10.2$ eV. As mentioned before, the real value should be smaller than this value because of the limited electron rearrangement during our transition-state calculation. Compared with Sec. V B, we believe the real value is in the currently accepted range of 7–9 eV.

Second, we calculated the electronic structure of six excited states: both nickel ions in the cluster have one $3d$ electron excited to an unoccupied $3d$ orbital. Table VIII gives the results of spin-up orbitals; the spin-down orbitals are the same except for the exchanging of atom 1 and

TABLE VII. Results of the four-atom Ni_2O_2 cluster with different atomic spin direction arrangement of surrounding atoms (the Ni_2O_2 cluster is in an antiferromagnetic state).

No.	Atomic spin direction arrangement	18 nearest Ni atoms up	18 nearest Ni atoms down	Total energy (K)	Energy gap (eV)	Abs. edge (eV)	Spin magnetic moment (μ_B) Ni_1 up	Spin magnetic moment (μ_B) Ni_2 down
1	antiferromagnet (31 up, 31 down)	9	9	0	0.510	4.129	1.9082	1.9082
2	disordered 1 (31 up, 31 down)	9	9	+360	0.507	4.110	1.9064	1.9056
3	disordered 2 (31 up, 31 down)	9	9	+261	0.509	4.124	1.9071	1.9063
4	disordered 3 (31 up, 31 down)	9	9	+193	0.510	4.134	1.9075	1.9067
5	disordered 4 (31 up, 31 down)	9	9	+193	0.507	4.119	1.9081	1.9065
6	disordered 5 (31 up, 31 down)	9	9	+185	0.510	4.124	1.9063	1.9070
7	disordered 6 (31 up, 31 down)	9	9	+164	0.510	4.124	1.9064	1.9080
8	disordered 7 (31 up, 31 down)	9	9	+212	0.508	4.120	1.9073	1.9059
9	all spins up (62 up, 0 down)	18	0	+161	0.524	4.153	1.9063	1.9082
10	special case (31 up, 31 down)	9	9	−280	0.512	4.140	1.9096	1.9096

atom 2. The results of six $3d$-$3d$ transitions involving the same nickel ion and the same spin direction (spin-keeping transitions) are reliable because the electron rearrangement is very small during the transitions (compared with the ground state in Table VIII, the changes of the eigenvalues are less than 0.02 Ry). In contrast, the result for state (8), in which both oxygen ions have one $2p$ electron excited to an unoccupied nickel $3d$ orbital, is not reliable because of the limitation of large electron rearrangement. We discuss the state (2): one $3d$ electron was transferred from orbital 36 to orbital 37, leaving a "hole" in the orbital 36. The excited orbital 37 (spin up) is mostly (98.5%) attached to the Ni_2 atom with only 1.0% hybridization to the Ni_1 atom and 0.2% hybridization to each oxygen atom. The overlap between two excited orbitals (orbital 37, spin up, attached to the Ni_2 atom; orbital 37, spin down, attached to the Ni_1 atom) is 1.85%. The overlap between the two holes is 2.89%. Figure 9(a) shows the charge distribution along the line connecting two nickel ions. It is clear that the nickel electrons are well localized and there is almost no overlap between the two nickel ions. The result for state (3) is similar. The overlap between the two excited orbitals is 4.17%, the overlap between the two holes is 3.46%. Figure 9(b) shows its charge distribution. Only three occupied nickel $3d$ orbitals (36, 35, and 34) have the same spin direction as the two unoccupied nickel $3d$ orbitals. Table VIII shows that the overlaps of the excited $3d$ orbitals are less than 4.5% and the overlaps of the holes are less than 6%. The spin-flipped $3d$-$3d$ transitions have much lower probabilities than that of spin-keeping transitions because they are dipole forbidden and they reduce the spin magnetic moment of the nickel ion to zero. The electron rearrangement in these transitions is large due to the disappearance of the spin magnetic moment of the nickel ion and the drastic change of exchange-correlation energy, which makes the result unreliable. Meanwhile, it is difficult to get a convergent result for a spin-flipped $3d$-$3d$ transition. Considering the results of spin-keeping transitions, we assume that for a spin-flipped $3d$-$3d$ transition,

TABLE VIII. Eigenvalues and Mulliken populations of the Ni_2O_2 cluster in eight states (spin-up orbitals).

State	Orbital No.	Occupation number	Eigenvalue (Ry)	Ni_1 (%)	Ni_2 (%)	O_1 (%)	O_2 (%)	Overlap (%)
	38	0	−0.2740	0.5	93.0	3.2	3.2	3.92
	37	0	−0.3243	1.1	98.1	0.3	0.3	2.10
	36(E_f)	1	−0.3618	0.1	97.3	1.3	1.3	2.98
(1)	35	1	−0.3669	1.4	96.3	1.2	1.2	4.53
ground	34	1	−0.4014	0.4	94.5	2.5	2.5	5.99
state	33	1	−0.4033	88.3	0.9	5.3	5.3	6.19
	32	1	−0.4583	96.3	2.3	0.6	0.6	4.73
	31	1	−0.4912	92.6	0.4	3.5	3.5	7.92
	30	1	−0.5001	95.3	1.1	1.8	1.8	5.92
	29	1	−0.5236	82.0	2.3	7.8	7.8	19.76
	28	1	−0.6278	17.3	2.9	39.9	39.9	84.48
(2)	37(exc.)	1	−0.3209	1.0	98.5	0.2	0.2	1.85
36 to 37	36(hole)	0	−0.3557	0.1	97.4	1.3	1.3	2.89
(3)	38(exc.)	1	−0.2755	0.6	92.6	3.4	3.4	4.17
36 to 38	36(hole)	0	−0.3642	0.1	96.8	1.5	1.5	3.46
(4)	37(exc.)	1	−0.3268	1.0	98.5	0.2	0.2	1.83
35 to 37	35(hole)	0	−0.3643	1.3	96.0	1.3	1.3	4.74
(5)	38(exc.)	1	−0.2849	0.5	92.3	3.5	3.5	4.37
35 to 38	35(hole)	0	−0.3759	1.3	96.0	1.4	1.4	4.93
(6)	37(exc.)	1	−0.3078	0.9	98.5	0.2	0.2	1.90
34 to 37	34(hole)	0	−0.3829	0.4	95.4	2.1	2.1	4.98
(7)	38(exc.)	1	−0.2624	0.5	93.0	3.2	3.2	4.02
34 to 38	34(hole)	0	−0.3878	0.4	94.6	2.5	2.5	5.91
	37(exc.)	1	0.0344	1.0	93.5	2.8	2.8	4.37
(8)	36	1	0.0014	87.1	−0.4	6.5	6.5	
28 to 37	35	1	−0.0026	0.5	98.1	0.6	0.6	
	28(hole)	0	−0.8266	0.2	0.2	49.8	49.8	99.94

the maximum overlap of an excited electron is the same as that of spin-keeping $3d$-$3d$ transition, and the maximum overlap of a hole is the same as that of the orbital in the ground state. Following this assumption, the overlaps of the holes in orbitals 30, 31, 32, and 33 are less than 8%, and the overlap of the hole in orbital 29 is less than 20%. The results for state (8) are not reliable. If the surrounding charge density ρ_2 can be fully rearranged, the eigenvalues of orbitals 35, 36, and 37 will become lower and the eigenvalues of orbital 28 will become higher. It is interesting to find that orbital 37 is still well localized (which means Ni^+ is localized), although we cannot confirm it absolutely. The only certain thing we can get from state (8) is that the overlap of the hole 28 is

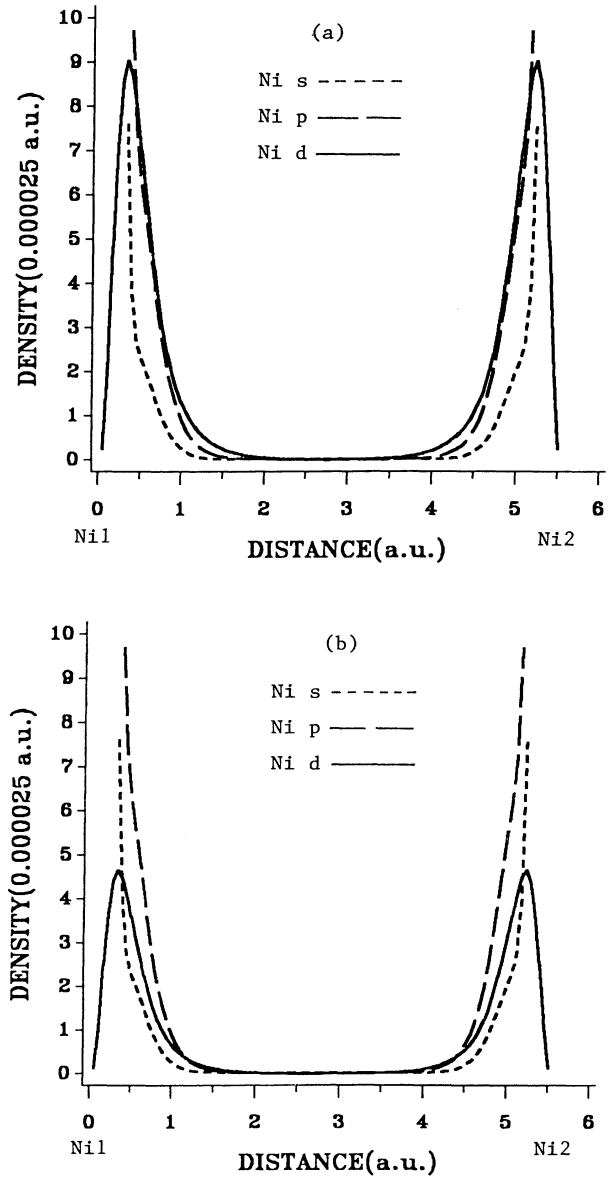

FIG. 9. The charge distribution along the line connecting two nickel ions. (a) Excited state 2. (b) Excited state 3.

larger than 84% because each hole is shared by two oxygen ions. In conclusion, similar to the ground state, the excited electrons and holes also have both localized and band properties. For all spin-keeping $3d$-$3d$ transitions, Table VIII shows that the overlaps of excited $3d$ orbitals are less than 4.5%, and the overlaps of $3d$ holes are less than 6%. For spin-flipped $3d$-$3d$ transitions, the overlaps of $3d$ holes may be less than 8% except for orbital 29, which may be about 20%. The holes in the oxygen $2p$ orbital are diffuse; the overlap is larger than 84%, which means the holes can move freely in the solid.

Now let us recall Mott's hydrogenic model.[17,19] For a simple lattice of hydrogen atoms with a *large* lattice constant, each electron should definitely be assigned to a particular site. The optimum configuration of a conducting state is one in which a single electron has been transferred from its "home site" to another site far away. The energy difference between the ground state and this excited configuration, to a first approximation, is the atomic ionization potential (13.6 eV) minus the electron affinity (0.75 eV): about 12.85 eV. So the ground state is clearly an insulating state.

We make two comments to the above argument. (i) If we calculate the electronic structure of such a hydrogenic model, to a first approximation, the energy gap will be 10.2 eV, the energy difference between the ground state and the first excited state. (ii) The above argument is valid only if this excited state is still localized and cannot form a metallic band. If the lattice constant is large enough, the excited orbital will definitely be localized and there is almost no overlap between the excited orbitals. Such a system has two energy gaps: one is the energy difference between the ground state and the first localized excited state, the other is the charge-transfer insulating gap. In a real material, if for some reason both the ground state and the first excited state are well localized and the overlaps are small enough, the material should have two energy gaps.

Consider the case of NiO. (i) The minimum energy required to transfer an electron from the nearest oxygen ion to a nickel site is about 4 eV (the main optical absorption edge). At least the hole left in the oxygen $2p$ bands can move freely in the solid. (ii) The minimum energy required to transfer a nickel $3d$ electron to an oxygen $3s$ conduction band is about 7 eV. (iii) The minimum energy required to transfer an electron from one nickel ion to another nickel ion far away is about 8 eV (the Hubbard U parameter for a nickel $3d$ electron). (iv) The $3d$ excited orbitals and holes of a nickel ion are well localized. For spin-keeping transitions, the overlaps of excited orbitals are less than 4.5%, and the overlaps of holes are less than 6%. For spin-flipped transitions, the overlaps of holes may be less than 8%, except for orbital 29, which may be about 20%.

Based on the argument above, we propose a new explanation for the insulating nature of NiO: The overlap of the excited $3d$ electrons is too small to form a metallic band, but the overlap is sufficient for the hole to migrate through the crystal by electron exchange. In this sense, NiO is a charge-transfer insulator with a gap of about 4 eV (mostly from oxygen to nickel). The calculated small

energy gap of 0.51 eV provides the activation energy, which is supported by the following experimental results.[11,48–52] The conductivity of NiO almost always increases exponentially with increasing temperature. The activation energy is about 0.2–0.9 eV. The Hall mobility is approximately 10^{-4}–0.5 cm^2/V sec and the predominant carriers are holes.

F. Discussion

We believe the calculation is reliable in the sense of the embedding procedure, the basis set, and the numerical calculation of V_{xc}. But our embedded cluster is small and contains only the 90° superexchange effect because of the computational limitation. Guo, Ellis, and Lam[9] have shown that the results of this method are converged when the size of the embedded cluster is increased. From the discussion in Sec. V A, we expect that the general picture will remain the same and the numerical values will be better compared with the experimental data if a big cluster containing both 90° and 180° arrangements of Ni ions is used. What we can confirm is that the ground state of NiO is an antiferromagnetic insulating state. NiO has both localized and band properties. Nickel $3d$ electrons are well localized and attached to a particular site. Oxygen $2p$ electrons are spread and form the bands. Nickel $3d$ levels are higher than oxygen $2p$ bands. Besides, the excited nickel $3d$ electrons and holes are also well localized. NiO remains an insulator when it transforms from antiferromagnetic to paramagnetic phase in which local AF order exists. This picture leads to a natural interpretation of almost all experimental data. We believe the self-consistent cluster-embedding method furnishes a reasonable starting point for describing the properties of NiO.

ACKNOWLEDGMENTS

The author particularly wishes to thank Professor J. Callaway for much instructive advice and for a critical reading of the manuscript. He is also indebted to Dr. H. Chen for his general free-cluster program package.

[1]Richard E. Watson, Phys. Rev. **11**, 1108 (1958).
[2]N. E. Brener and J. Callaway, Phys. Rev. B **35**, 4001 (1987).
[3]H. Chen and J. Callaway, Phys. Rev. B **40**, 8800 (1989); **44**, 2289 (1991).
[4]Y. Guo, J. M. Langlois, and W. A. Goddard III, Science **239**, 896 (1988).
[5]R. L. Martin, in *Cluster Models for Surface and Bulk Phenomena, NATO Advanced Study Institute Series B: Physics,* edited by G. Pacchiomi and P. S. Bagus (Plenum, New York, 1991).
[6]D. E. Ellis, G. A. Benesh, and E. Byrom, Phys. Rev. B **16**, 3308 (1977); **20**, 1198 (1979).
[7]S.-H. Chou, J. Guo, and D. E. Ellis, Phys. Rev. B **34**, 12 (1986).
[8]D. E. Ellis and D. J. Lam, Physica B **150**, 25 (1988).
[9]J. Guo, D. E. Ellis, and D. J. Lam, Phys. Rev. B **45**, 3204 (1992).
[10]J. E. Inglesfield, J. Phys. C **14**, 3795 (1981).
[11]David Adler and Julius Feinleib, Phys. Rev. B **2**, 3112 (1970).
[12]T. Oguchi, K. Terakura, and A. R. Williams, Phys. Rev. B **28**, 6443 (1983).
[13]T. Oguchi, K. Terakura, and A. R. Williams, J. Appl. Phys. **55**, 2318 (1984).
[14]K. Terakura, A. R. Williams, T. Oguchi, and J. Kubler, Phys. Rev. Lett. **52**, 1830 (1984).
[15]K. Terakura, T. Oguchi, A. R. Williams, and J. Kubler, Phys. Rev. B **30**, 4734 (1984).
[16]P. W. Anderson, Phys. Rev. **115**, 2 (1959).
[17]N. F. Mott, Proc. Phys. Soc. London Sec. A **62**, 416 (1949).
[18]J. Hubbard, Proc. R. Soc. London Ser. A **276**, 238 (1963).
[19]B. H. Brandow, Adv. Phys. **26**, 651 (1977).
[20]A. Fujimori, F. Minami, and S. Sugano, Phys. Rev. B **29**, 5225 (1984).
[21]A. Fujimori and F. Minami, Phys. Rev. B **30**, 957 (1984).
[22]G. A. Sawatzky and J. W. Allen, Phys. Rev. Lett. **53**, 2339 (1984).
[23]Z.-X. Shen *et al.*, Phys. Rev. B **44**, 3604 (1991).
[24]P. Hohenberg and W. Kohn, Phys. Rev. **136**, B864 (1964).
[25]W. Kohn and L. J. Sham, Phys. Rev. **140**, A1133 (1965).
[26]H. Chen, Ph.D. thesis, Louisiana State University, 1988 (unpublished).
[27]A. J. H. Wachters, J. Chem. Phys. **52**, 1033 (1970).
[28]F. B. van Duijneveldt (unpublished).
[29]A. K. Rappe, T. A. Smedley, and W. A. Goddard III, J. Phys. Chem. **85**, 2607 (1981).
[30]S. Huzinaga, *Gaussian Basis Sets for Molecular Calculations* (Elsevier, New York, 1984).
[31]U. von Barth and L. Hedin, J. Phys. C **5**, 1629 (1972).
[32]A. K. Rajagopal, S. Singhal, and J. Kimball (unpublished) as quoted by A. K. Rajagopal, in *Advances in Chemical Physics,* edited by G. I. Prigogine and S. A. Rice (Wiley, New York, 1979), Vol. 41, p. 59.
[33]R. W. G. Wyckoff, *Crystal Structures* (Interscience, New York, 1965), Vol. 1.
[34]C. Kittel, *Introduction to Solid State Physics,* 5th ed. (Wiley, New York, 1976).
[35]C. G. Shull, W. A. Strauser, and E. O. Wollan, Phys. Rev. **83**, 333 (1951).
[36]B. E. F. Fender, A. J. Jacobson, and F. A. Wegwood, J. Chem. Phys. **48**, 990 (1968).
[37]H. A. Alperin, J. Phys. Soc. Jpn. Suppl. B **17**, 12 (1962).
[38]A. K. Cheetham and D. A. O. Hope, Phys. Rev. B **27**, 6964 (1983).
[39]A. Svane and O. Gunnarson, Phys. Rev. Lett. **65**, 1148 (1990).
[40]S. Hufner, J. Osterwalder, T. Riesterer, and F. Hulliger, Solid State Commun. **52**, 793 (1984).
[41]H. A. Kramers, Physica **1**, 182 (1934).
[42]P. W. Anderson, Phys. Rev. **79**, 350 (1950); **79**, 705 (1950).
[43]J. F. Janak, Phys. Rev. B **18**, 7165 (1978).
[44]J. C. Slater and J. H. Wood, Int. J. Quantum Chem. Symp. **4**, 3 (1971).
[45]J. C. Slater, Adv. Quantum Chem. **6**, 1 (1972).
[46]R. J. Powell and W. E. Spicer, Phys. Rev. B **2**, 2182 (1970).
[47]V. A. Gubanov and D. E. Ellis, Phys. Rev. Lett. **44**, 1633 (1980).
[48]S. Koide, J. Phys. Soc. Jpn. **20**, 123 (1965).
[49]I. G. Austin, A. J. Springthorpe, B. A. Smith, and C. E. Turner, Proc. Phys. Soc. **90**, 157 (1967).
[50]H. J. van Daal and A. J. Bosman, Phys. Rev. **158**, 736 (1967).
[51]J. E. Keem, J. M. Honig, and L. L. van Zandt, Philos. Mag. B **37**, 537 (1978).
[52]J. E. Keem and M. A. Wittenauer, Solid State Commun. **26**, 213 (1978).